JJMIE

Volume 20, Number 1, March. 2026
ISSN 1995-6665
Pages 37– 47
https://doi.org/10.59038/jjmie/200104
Editor-in-Chief: Prof. Faris M. AL-Oqla

Jordan Journal of Mechanical and Industrial Engineering

Multi-Response Optimization of EDM Parameters for Nano-ZrO_2 Reinforced Aluminum Matrix Composites Using Taguchi–Grey Relational Analysis

Sattar Hantosh A. Alfatlawi[1], Fatma Hentati[2*], Neila Masmoudi Khabou[3]

[1] College of Material's Engineering, University of Babylon, Iraq.
[2]Applied Mechanics and Engineering Laboratory (LR-MAI), National Engineering School of Tunis ENIT, Tunis, 1002, Tunisia.
[3] Electromechanical Systems Laboratory (LASEM), National Engineering School of Sfax, University of Sfax, Tunisia BP 1173 3038.

Received 20 Jul 2025 Accepted 1 Feb 2026

Abstract

This study investigates the elaboration of aluminum matrix composites reinforced with nano-sized zirconium dioxide (ZrO_2) particles (25 ± 5 nm) fabricated via the stir casting technique and evaluates their machinability using Electric Discharge Machining (EDM). The Taguchi method, based on an L9 orthogonal array, was employed to analyze and optimize the EDM process by examining the effect of three process parameters: peak intensity (IP), pulse-on time (TON), and pulse-off time (TOFF), each at three levels. Material removal rate (MRR), tool wear rate (TWR), and surface roughness (Ra) were selected as the primary performance responses. Signal-to-noise (S/N) ratio analysis was applied using the "Larger-is-Better" criterion for MRR and the "Smaller-is-Better" criterion for TWR and Ra. To obtain a single optimal machining condition considering all responses simultaneously, Grey Relational Analysis (GRA) was employed. The results indicate that peak intensity is the most influential parameter affecting all output responses, particularly MRR. The combined Taguchi–GRA approach identified the optimal EDM parameters as IP = 14 A, TON = 60 µs, and TOFF = 20 µs, yielding improved machining efficiency with reduced tool wear and acceptable surface quality. The findings demonstrate that nano-ZrO_2 reinforcement significantly enhances the EDM machinability of aluminum-based composites. These results are of practical relevance for industrial applications requiring high machining efficiency and reliable surface integrity, particularly in marine, structural, and corrosion-resistant components.

Keywords: Aluminum matrix, Nano-zirconium oxide, Electric Discharge Machining, Taguchi method, Optimization.

1. Introduction

The advancement of materials with optimized properties plays a crucial role in satisfying the complex demands of contemporary industrial applications. Aluminum alloys have attracted considerable interest due to their lightweight nature, excellent thermal and electrical conductivity, and resistance to corrosion and saline environments. Consequently, aluminum matrix composites (AMCs) have gained prominence across diverse sectors, including aerospace, automotive, and marine engineering [1]. Various fabrication techniques, including stir casting, pressure-assisted casting methods, and powder metallurgy, are employed to produce AMCs. Among these methods, stir casting is widely employed thanks to its cost-effectiveness, simplicity, and ability to achieve relatively uniform distribution of reinforcement particles. Composites produced through this method generally exhibit favorable mechanical characteristics, including adequate hardness, density, and low porosity [2]. Recent systematic reviews further highlight the continuous advancements in metal matrix composites fabrication, pointing to improved strength, wear resistance, and adaptability achieved through optimized processing methods and reinforcements [3]. Several studies have focused on enhancing AMCs properties by incorporating ceramic and natural reinforcements, thereby improving performance in demanding industrial environments [4,5]. For instance, silicon nitride (Si_3N_4) reinforced AMC fabricated via stir casting demonstrated significant improvements in ultimate tensile strength and microhardness [6]. Similarly, titanium carbide (TiC) reinforcement in Al5052 alloy enhanced mechanical properties, although excessive brittle additions can lead to crack formation [7]. The integration of ceramic reinforcements such as Al_2O_3, TiC, SiC, $ZrSiO_4$, and B_4C has been reported to improve both mechanical and tribological performance [8], while unidirectional carbon fibers have been used to increase yield strength, tensile strength, and Young's modulus [9]. More recent work has shown that hybrid and nano-scale reinforcements can further boost composite performance, including machinability behavior when processed with non-traditional methods like wire-cut EDM [10].

* Corresponding author e-mail: fatma.hentati1@gmail.com.

Stir Casting has also enabled the development of AA5052 aluminum matrix composites reinforced with nano-ceramic particles, including nano-Al_2O_3, nano-TiO_2, and nano-ZrO_2 [11]. Reinforcing aluminum matrices with alumina and bauxite particles has shown notable improvements in hardness, wear resistance, and microstructural integrity [12]. The addition of nano-graphene and ZrO_2 has further been reported to enhance particle distribution and mechanical strength [13]. Other studies investigated aluminum matrices reinforced with ZrO_2 and Al_2O_3 (5–10 wt.% Al and 8 wt.% ZrO_2) using stir casting, evaluating wear performance via Taguchi L_9 orthogonal array and ANOVA analysis [14]. Aluminum-silicon alloys reinforced with ZrO_2 were assessed for tensile strength, hardness, and compressive strength across different fabrication techniques [15]. Additionally, investigations on drilling performance of Al6061/Al6063 composites reinforced with SiC and ZrO_2 have provided insights into microstructure–machinability relationships under multi-criteria optimization [16]. The influence of ZrO_2 on Al7075 alloy produced through compo casting also showed notable enhancements in tensile strength and hardness [17]. Electric Discharge Machining (EDM) has become an effective non-conventional technique for machining hard and electrically conductive materials that are difficult to process using traditional methods [18]. Several studies have demonstrated the successful application of EDM to aluminum matrix composites reinforced with ceramic particles, such as alumina-reinforced AMCs, where material removal rate (MRR) and tool wear rate (TWR) were systematically evaluated using Taguchi-based experimental designs [19]. Aluminum composites reinforced with titanium boride (TiB_2) have also been efficiently machined by EDM despite their high hardness and abrasive nature [20]. In addition, the machining performance of Al5052 alloys has been optimized through EDM by identifying suitable combinations of electrical input parameters [21]. More recent investigations highlight the effectiveness of advanced multi-response optimization techniques, including hybrid approaches that integrate Taguchi methods, Grey Relational Analysis (GRA), and artificial intelligence tools, to simultaneously optimize multiple EDM performance characteristics. In particular, the Taguchi–GRA approach has been successfully employed to optimize surface roughness and tool wear in aluminum-based composites [22,23], while multi-objective GRA-based frameworks have been applied to EDM of aluminum hybrid composites and Al alloys to achieve balanced improvements in MRR, TWR, and surface quality [24–27]. Furthermore, studies on alumina–zirconia (Al_2O_3/ZrO_2) ceramic composites have shown that, despite their brittle nature, EDM combined with assistive electrode mechanisms can significantly enhance dimensional accuracy and increase MRR under higher energy input conditions [28].

Nevertheless, the effect of nano-sized ZrO_2 reinforcement on the machinability of aluminum matrices under EDM is not fully understood, particularly when aiming to optimize multiple outputs such as MRR, TWR, and surface roughness Ra simultaneously. Moreover, while previous studies have applied Taguchi methods for EDM optimization, few have addressed the systematic integration of nano reinforcements with multi-response optimization, which is critical for industrial applications. In response to this unexplored area, aluminum matrix composites reinforced with nano-ZrO_2 ($25^{\pm5}$ nm) were fabricated via stir casting, and their EDM performance was systematically investigated. A Taguchi L_9 orthogonal array design was employed to optimize machining parameters, including peak intensity (I_P), pulse-on time (T_{ON}), and pulse-off time (T_{OFF}). The study aims to identify optimal machining conditions, improve understanding of nano-ZrO_2's contribution to machining efficiency, and provide a framework for industrial applications where precision and material performance are critical. This research provides novel insights into the synergistic effects of nanoscale reinforcement and process optimization, resulting in enhanced mechanical properties and machinability of aluminum-based nanocomposites.

2. Experimental Protocol

2.1. Preparation of Aluminum Matrix Composites

Aluminum matrix composites were fabricated with different percentages of nano-zirconium dioxide (ZrO_2) particles (6, 7, and 8 wt.%). The aluminum melt was prepared in a graphite crucible at 675 °C using the stir casting method after the aluminum was properly cleaned. Slag was removed from the melt, and nano-ZrO_2 particles ($25^{\pm5}$ nm) were added. The molten mixture was stirred continuously at 750 rpm using an electric mixer, with intermittent pauses to ensure homogeneous dispersion and uniform particle distribution.

Magnesium (2 wt.%) was added to the melt to improve wetting and enhance the adhesion between the aluminum matrix and the reinforcement particles. Prior to addition, the nano-ZrO_2 particles were wrapped in aluminum foil and preheated at 200 °C for 10 minutes to remove moisture. The melt temperature was initially lowered during mixing and then raised to 850 °C to prevent particle agglomeration and increase fluidity. Reinforcements were gradually incorporated into the vortex of the molten aluminum under continuous stirring. The composite melt was then poured into preheated cast iron molds after final slag removal and allowed to solidify at room temperature to form the metallic composite samples. Based on preliminary trials and previous studies [11,19], a reinforcement content of 7 wt.% was selected as optimal. Lower content (6 wt.%) resulted in visible casting defects, while higher content (8 wt.%) caused increased brittleness and higher vibration during the EDM process.

Cylindrical samples with a diameter of 12 mm and a height of 8 mm were prepared using a conventional lathe machine for subsequent EDM experiments.

2.2. EDM Process and Experimental Design

Electric Discharge Machining (EDM) was performed on the prepared composite samples using a CHMER 50N machine. Surface roughness measurements (Ra) were taken after machining using a surface roughness tester (HSR210). EDM operates based on electrical discharges occurring across a small gap (approximately 10 mm) between the electrode (tool) and the workpiece (sample), causing localized melting and vaporization of material.

The machining process is governed by several input parameters, namely peak intensity (I_P), pulse-on time (T_{ON}), and pulse-off time (T_{OFF}). In this study, the machining performance was evaluated using four output responses: material removal rate (MRR), tool wear rate (TWR), surface roughness (Ra). Based on preliminary experiments and relevant literature [11,19], three levels were selected for

each input parameter: peak intensity of 10, 12, and 14 A; pulse-on time of 30, 60, and 90 μs; and pulse-off time of 20, 40, and 60 μs. The selected machining parameters and their corresponding levels are summarized in Table 1.

The output parameters MRR and TWR were calculated using the following equations:

$$MRR = \frac{w_i - w_f}{\rho \cdot T} \quad (1)$$

$$TWR = \frac{w_{ti} - w_{tf}}{\rho \cdot T} \quad (2)$$

Where: w_i , w_{ti} , w_f and w_{tf} are the weights of the sample and tool before and after machining.

ρ : is the material density.

T: is machining time.

The density of the copper tool was 8.9 g/cm³ (length: 90 mm, diameter: 10 mm), while the density of the composite samples, measured via the Archimedes method, was 2.624 g/cm³.

Table 1. EDM input parameters and their experimental levels.

Levels	Trial nº	I_P (A)	T_{ON}(μs)	T_{OFF} (μs)
Level 1	1	10	30	20
	2	10	60	40
	3	10	90	60
Level 2	4	12	30	40
	5	12	60	60
	6	12	90	20
Level 3	7	14	30	60
	8	14	60	20
	9	14	90	40

Accordingly, the experimental design was developed using the Taguchi method with three input parameters, each evaluated at three levels, resulting in a total of nine experimental runs based on the L_9 orthogonal array. In this study, the "Larger-is-Better" criterion was adopted for maximizing the material removal rate (MRR), whereas the "Smaller-is-Better" criterion was applied for minimizing the tool wear rate (TWR) and surface roughness (Ra). Prior to each machining trial, both the tool electrode and the workpiece were weighed, after which the selected EDM input parameters, including voltage, spark gap, peak intensity (I_P), pulse-on time (T_{ON}), and pulse-off time (T_{OFF}), were set.

Upon completion of each machine operation, the machining time was recorded, and the tool and workpiece were reweighed to determine the corresponding weight loss. This procedure was repeated for all nine experimental runs, and each experimental condition was replicated a minimum of three times to improve statistical reliability. Surface roughness measurements were taken at multiple locations on each machined surface, and the average Ra value was reported. The EDM performance results obtained are summarized in Table 2. These steps were repeated for all nine experimental runs according to the L_9 orthogonal array. For each run, the machining time and tool weight loss were recorded. Surface roughness measurements were performed at multiple locations on each sample, and the average Ra value was reported.

Table 2. Experimental results of EDM output parameters.

Levels	Trial nº	MRR (mm^3/min)	TWR (mm^3/min)	Ra(μm)
Level 1	1	9.6203	0.0232	1.725
	2	9.5521	0.0201	1.833
	3	10.0065	0.0197	2.002
Level 2	4	11.0341	0.0203	2.102
	5	10.8388	0.0294	4.248
	6	16.3115	0.0311	2.041
Level 3	7	14.9073	0.0381	2.118
	8	21.2178	0.0465	2.315
	9	20.2633	0.0437	4.396

2.3. Flow Chart of the EDM Process

Figure 1 illustrates the experimental methodology adopted for the fabrication and machining of an AA5052–ZrO_2 metal matrix composite and the subsequent evaluation of its machining performance. Pure aluminum (91 wt.%), magnesium (2 wt.%), and nano-sized zirconium dioxide particles (7 wt.% ZrO_2) were used as the base materials. The composite was synthesized using a stir casting technique, carried out at a processing temperature of 675 °C with a stirring speed of 750 rpm to ensure homogeneous dispersion of the reinforcement particles within the aluminum matrix. The cast composite was produced in cylindrical specimens with a diameter of 12 mm and a height of 8 mm. These specimens were then subjected to Electrical Discharge Machining (EDM). Process parameters, including peak intensity (I_P), pulse-on time (T_{ON}), and pulse-off time (T_{OFF}), were selected based on the Taguchi method to systematically study their influence on machining performance.

The machining outputs evaluated were material removal rate (MRR) and tool wear rate (TWR). Additionally, surface integrity was assessed by measuring surface roughness (Ra) using a roughness tester. This structured methodology enables a comprehensive assessment of the effects of EDM process parameters on the machinability and surface quality of the AA5052–ZrO_2 nanocomposite.

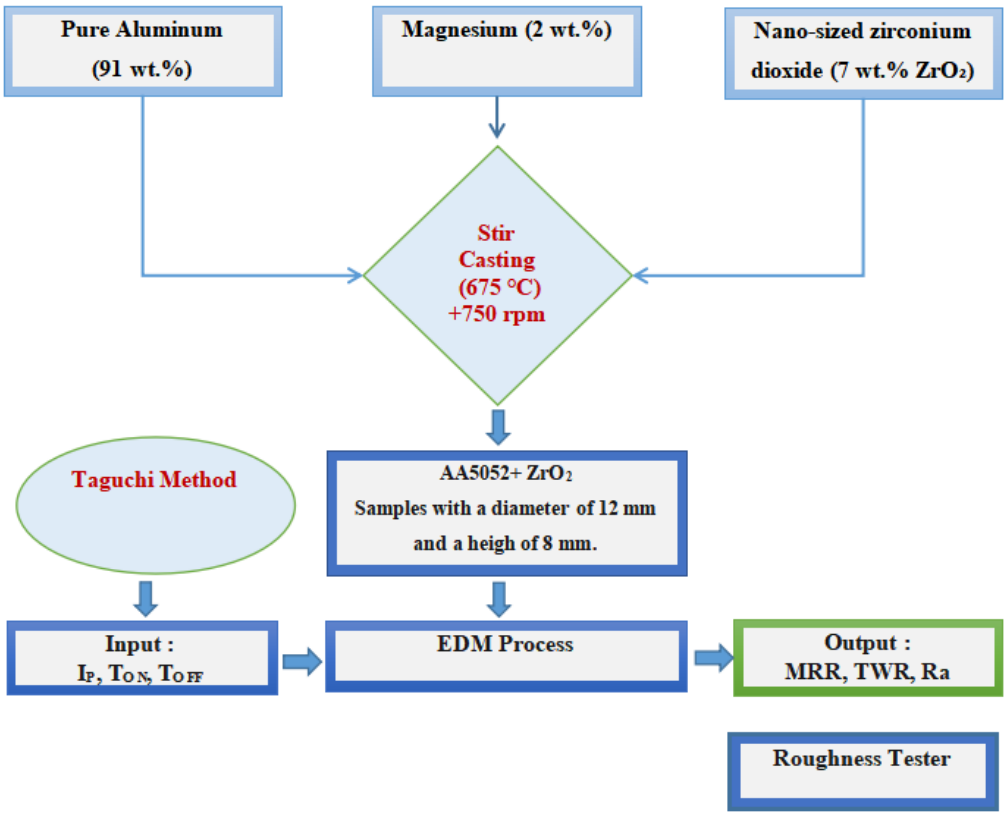

Figure 1. Process flow of stir casting and EDM of AA5052–ZrO_2 composite.

3. Results and Discussion

3.1. Taguchi Approach

The application of design of experiments (DOE) techniques provides an efficient means to reduce the number of required trials while systematically identifying the key factors influencing product quality. DOE has been widely adopted to optimize process parameters across diverse engineering applications [29–34]. Among these techniques, the Taguchi method is particularly effective due to its structured use of orthogonal arrays and the signal-to-noise (S/N) ratio, which evaluates process robustness by considering both the mean response and its variability [33–37]. A higher S/N ratio indicates that the system's output is dominated by the desired signal rather than by uncontrollable noise. Accordingly, maximizing the S/N ratio is essential for improving process stability.

In this study, the Taguchi L_9 orthogonal array was employed to investigate the influence of three EDM input parameters: peak intensity (I_P), pulse-on time (T_{ON}), and pulse-off time (T_{OFF}), each evaluated at three levels, resulting in a total of nine experimental runs. The signal-to-noise (S/N) ratio is a central concept in the Taguchi method, used to quantify the robustness of a process by considering both the mean and variability of a response. The same S/N ratio formula is applied for all types of responses; what differs is how the response values $Y_i$are treated depending on whether higher or lower values are desirable. S/N ratio was used to determine the optimal levels of each parameter for the responses: material removal rate (MRR), tool wear rate (TWR), and surface roughness (Ra). Specifically, the "Larger-is-Better" (LTB) criterion was applied for MRR, whereas the "Smaller-is-Better" (STB) criterion was used for TWR and Ra. Thus, S/N ratios were calculated as follows:

$$S/N_{ratio} = -10\log\frac{1}{n}\sum_{i=1}^{n}Y_i^2 \quad (3)$$

Where:

n: is the total number of experimental trials.

Y_i: is the response value obtained from the i^{th} experiment.

In the present study, the Taguchi method was employed to evaluate the effects of three key EDM parameters: peak intensity (I_P), pulse-on time (T_{ON}), and pulse-off time (T_{OFF}) on material removal rate (MRR), tool wear rate (TWR), and surface roughness (Ra). The primary objective was to determine the optimal combination of these parameters to improve machining performance. Statistical analysis and optimization were carried out using MINITAB 19 software, and a confirmation experiment was conducted to validate the results under the optimal settings identified from the Taguchi analysis. The input parameters and their three-level values are summarized in Table 3. The experimental design followed an L_9 orthogonal array, resulting in a total of nine tests.

Table 3. Process parameters and their levels.

Symbol	Process parameters	Unit	Level 1	Level 2	Level 3
A	**I_P**	**A**	10	12	14
B	**T_{ON}**	**µs**	30	60	90
C	**T_{OFF}**	**µs**	20	40	60

The study investigated three key EDM process parameters: peak intensity (I_P, A), pulse-on time (T_{ON}, B),

and pulse-off time (T_{OFF}, C), each evaluated at three levels as shown in Table 1. The degrees of freedom (DOF) for each parameter were calculated as the number of levels minus one (DOF = 3 − 1). Table 4 presents the L_9 orthogonal array generated using MINITAB 19 software, detailing the nine experimental runs designed according to the Taguchi methodology.

Table 4. L_9 Orthogonal array-based design of control factors.

Combination tests	I_P (A)	T_{ON} (µs)	T_{OFF} (µs)
C_1	1	1	1
C_2	1	2	2
C_3	1	3	3
C_4	2	1	2
C_5	2	2	3
C_6	2	3	1
C_7	3	1	3
C_8	3	2	1
C_9	3	3	2

3.2. Evaluation of Material Removal Rate (MRR)

The study investigated the effects of three EDM process parameters: peak intensity (I_P, A), pulse-on time (T_{ON}, B), and pulse-off time (T_{OFF}, C) each evaluated at three levels (Table 5). The influence of these factors on material removal rate (MRR) was assessed using both the main effects and signal-to-noise (S/N) ratios, calculated according to Eq. (3) using the "Larger-is-Better" criterion.

3.2.1. Main Effects of Process Parameters

The influence of peak intensity (IP, A), pulse-on time (TON, B), and pulse-off time (TOFF, C) on material rate removal (MMR) were evaluated using both main responses and signal-to-noise (S/N) ratios, calculated according to Eq. (3) using the "Larger-is-Better" criterion. Table 5 summarizes these results, including the mean responses at each parameter level and the corresponding standard deviations for each experiment.

Table 6 presents the average MRR values for each level of the process parameters, while Figure 2 illustrates the main effects plots. The results show that MRR increases with higher peak intensity and pulse-on time (T_{ON}, B) but decreases with increasing pulse-off time (T_{OFF}, C). The ranking of parameter influence, based on the range of average MRR values, indicates that peak intensity (I_P, A) has the most significant effect, followed by pulse-off time (T_{OFF}, C) and pulse-on time (T_{ON}, B).

Table 5. Experimental results based on L_9 orthogonal array.

Combination tests	I_P (A)	T_{ON} (µs)	T_{OFF} (µs)	MRR (mm^3/min)	S/N
C_1	1	1	1	9.62	19.67
C_2	1	2	2	9.55	19.6
C_3	1	3	3	10	20
C_4	2	1	2	11	20.86
C_5	2	2	3	10.83	20.7
C_6	2	3	1	16.31	24.25
C_7	3	1	3	14.9	23.46
C_8	3	2	1	21.21	26.53
C_9	3	3	2	20.26	26.13

$\overline{MRR}$: Material removal rate = 13.75 mm^3/min.

Table 6. Main effects of process parameters on average MRR.

Levels	Material Removal Rate MRR (mm^3/min)		
	A	B	C
L_1	9.73	11.85	15.72
L_2	12.73	13.87	13.62
L_3	18.8	15.53	11.92
Min-Max	9.07	3.67	3.8
Rank	1	3	2

The main effects plot in Figure 2 indicates that the optimal parameter combination for higher MRR values is A3 (14 A), B3 (90 µs), and C1 (20 µs). Thus, the optimal parameter combination for maximizing MRR is A3, B3, and C1. Furthermore, Figure 2 shows that peak intensity (I_P), represented by parameter A, has the most significant effect on MRR compared to the other parameters.

3.2.2. Signal to Noise ratio (S/N)

The signal-to-noise (S/N) ratios for material removal rate (MRR), obtained from the L_9 orthogonal array experiments, are presented in Table 7. Analysis of these ratios indicates that peak intensity (I_P) has the greatest influence on MRR, followed by pulse-on time (T_{ON}), with pulse-off time (T_{OFF}) having the least effect. These findings, also illustrated in Figure 3, are consistent with the main effects analysis.

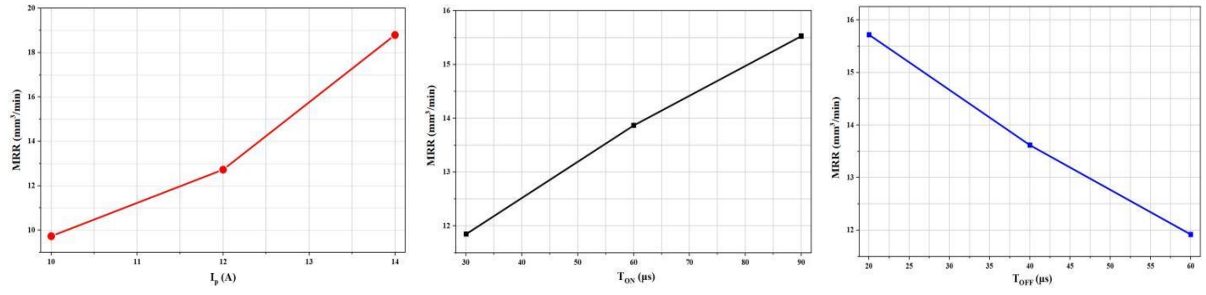

(a) **(b)** **(c)**

Figure 2. Main effect of process parameters: **(a)** peak Intensity I_P, **(b)** pulse-ON Time (T_{ON}) and **(c)** pulse-OFF Time (T_{OFF}) on MRR.

Table 7. Signal-to-Noise (S/N) ratio analysis for MRR.

Levels	Material Removal Rate MRR (mm³/min)		
	A	B	C
L_1	19.76	21.33	23.48
L_2	21.93	22.28	22.20
L_3	25.38	23.46	21.39
Min-Max	5.62	2.13	2.09
Rank	1	2	3

The S/N ratio analysis confirms that the A3, B3, and C1 parameter combination maximizes MRR while minimizing process variability, as shown in Figure 3.

The factor level combination (3, 3, 1) presented in Table 3 differs from those derived from the initial main effects analysis, emphasizing the need to identify the precise optimal parameter settings. A full factorial experimental design would typically involve 81 runs, but the Taguchi method reduces this to just 9, greatly improving efficiency. Since the optimal combination was not included in the initial set of experiments, additional confirmation tests were conducted to validate the proposed optimal conditions.

3.2.3. Estimation of Predicted Means and Experimental Validation

The predicted mean is estimated to confirm the effectiveness of the optimal parameter levels A3, B3, and C1 in maximizing the material removal rate (MRR). The calculation of the predicted mean (w) is based on the following equation [38-41]:

$$W_{MRR} = \overline{MRR} + (\overline{A_3} - \overline{MRR}) + (\overline{B_3} - \overline{MRR}) + (\overline{C_1} - \overline{MRR}) \quad (4)$$

Here, A3 represents the average MRR at the third level of I_P, B3 denotes the average MRR at the third level of T_{ON}, and C1 indicates the average MRR at the first level of T_{OFF} (see Table 6).

$\overline{MRR}$ is the mean of MRR (Table 3). Applying the values to the terms in Eq. (4).

The optimal process parameters suggested by this study were validated through three confirmation experiments for each response. The average material removal rate (MRR) recorded under these conditions was 8.79 mm³/min. The deviation of 0.63% between the predicted and observed values suggests that the variation is not significant. Consequently, the experimental results fall within the confidence interval of the predicted MRR, as presented in Table 8.

Table 8. Confirmation results.

	Computed value	Confirmation value	Deviation (%)
MRR (mm³/min)	8.79	9.42	0.63

3.3. Evaluation of Tool Wear Rate (TWR) and Surface Roughness (Ra)

3.3.1. Main Effects of Process Parameters

The effects of peak intensity (I_P, A), pulse-on time (T_{ON}, B), and pulse-off time (T_{OFF}, C) on tool wear rate (TWR) and surface roughness (Ra) were evaluated using both main responses and signal-to-noise (S/N) ratios, calculated according to Eq. (3) using the "Smaller-is-Better" criterion. Table 9 summarizes the experimental results for the nine L_9 orthogonal array runs.

Table 10 summarizes the average values of tool wear rate (TWR) and surface roughness (Ra) for parameters A, B, and C at their respective levels 1, 2, and 3. The main effects and their variations across these parameter levels are illustrated in the response plots shown in Figures 3 and 4. For each level, the average response was calculated by taking the mean of the results from all corresponding trials. The primary goal of this study is to achieve the "Smaller-is-Better" quality characteristic by optimizing the process parameters accordingly.

Table 9. Experimental results based on L_9 orthogonal array design.

Combination tests	I_P (A)	T_{ON} (µs)	T_{OFF} (µs)	TWR (mm³/min)	S/N	Ra (µm)	S/N
C_1	1	1	1	0.023	32.7	1.72	-4.76
C_2	1	2	2	0.02	33.94	1.83	-5.27
C_3	1	3	3	0.019	34.11	2	-6.03
C_4	2	1	2	0.02	33.85	2.1	-6.45
C_5	2	2	3	0.029	30.63	4.24	-12.57
C_6	2	3	1	0.031	30.15	2	-6.2
C_7	3	1	3	0.038	28.39	2.11	-6.52
C_8	3	2	1	0.046	26.65	2.31	-7.29
C_9	3	3	2	0.043	27.19	4.39	-12.87

$\overline{TWR}$: Tool Wear Rate = 0.029 mm³/min.

$\overline{Ra}$: Roughness = 2.52 µm.

Table 10. Main effects of process parameters on average TWR and Ra.

Levels	TWR (mm³/min)			Ra (µm)		
	A	B	C	A	B	C
L_1	0.021	0.027	0.034	1.85	1.99	2.027
L_2	0.027	0.032	0.028	2.8	2.8	2.777
L_3	0.042	0.031	0.029	2.95	2.8	2.789
Min-Max	0.021	0	0	1.1	0.831	0.762
Rank	1	3	2	1	2	3

Table 10 presents the main responses TWR and Ra values for each parameter level, while Figures 4 and 5 show the corresponding main effects plots. The results indicate that peak intensity (I_P) has the most significant influence on both TWR and Ra, followed by pulse-off time (T_{OFF}) and pulse-on time (T_{ON}).

The tool wear rate (TWR) increases under low peak intensity I_P (10 A) and pulse-on time (T_{ON}, 30 µs) conditions, reaching a maximum at the second level of pulse-off time T_{OFF} (40 µs). Therefore, the parameter combination A1, B1, C2 is identified as the optimal for minimizing TWR. Conversely, surface roughness (Ra) exhibits its maximum values at low: peak intensity I_p (10 A), pulse-on time T_{ON} (30 µs), and pulse-off time T_{OFF} (20 µs). The optimal combination for minimizing Ra is therefore approximately A1, B1, C1.

3.3.2. Signal to Noise ratio (S/N)

Using the L_9 orthogonal array, experimental measurements of TWR and Ra yielded the S/N ratios listed in Table 11. Analysis of the S/N ratios and associated ranking of each control parameter demonstrates that I_P parameter exerts the greatest influence on TWR, followed by T_{OFF} and T_{ON}, in decreasing order of significance. For Ra response, I_P represents the most important factor followed by T_{ON} and T_{OFF}.

The S/N analysis confirms the parameter levels that yield the optimal TWR, as depicted in Figure 6. Accordingly, the levels A3, B2, and C1 have been determined to be the most effective.

Similarly, the S/N analysis for the Ra response, shown in Figure 7, indicates that the optimal parameter levels are A3, B2, and C3.

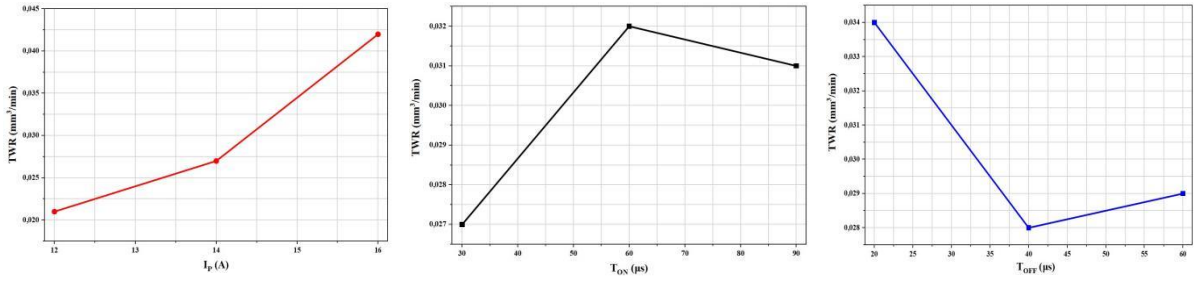

(a) **(b)** **(c)**

Figure 4. Main effect of process parameters: **(a)** peak Intensity I_P, **(b)** pulse-ON Time (T_{ON}) and **(c)** pulse-OFF Time (T_{OFF}) on TWR.

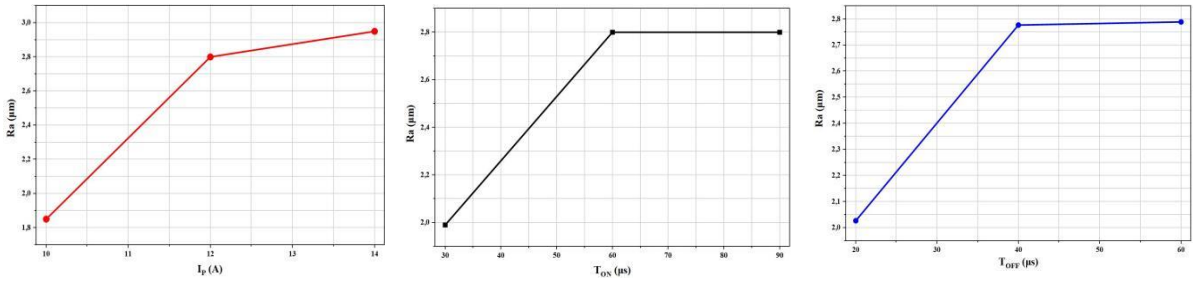

(a) **(b)** **(c)**

Figure 5. Main effect of process parameters: **(a)** peak Intensity I_P, **(b)** pulse-ON Time (T_{ON}) and **(c)** pulse-OFF Time (T_{OFF}) on Ra.

Table 11. Responses table for S/N ratios.

Levels	TWR (mm³/min)			Ra (µm)		
	A	B	C	A	B	C
L_1	33.58	31.64	29.83	-5.343	-5.9	-6.07
L_2	31.54	30.41	31.66	-8.4	-8.37	-8.19
L_3	27.41	30.48	31.04	-8.89	-8.36	-8.37
Min-Max	6.17	1.23	1.83	3.54	2.47	2.29
Rank	1	3	2	1	2	3

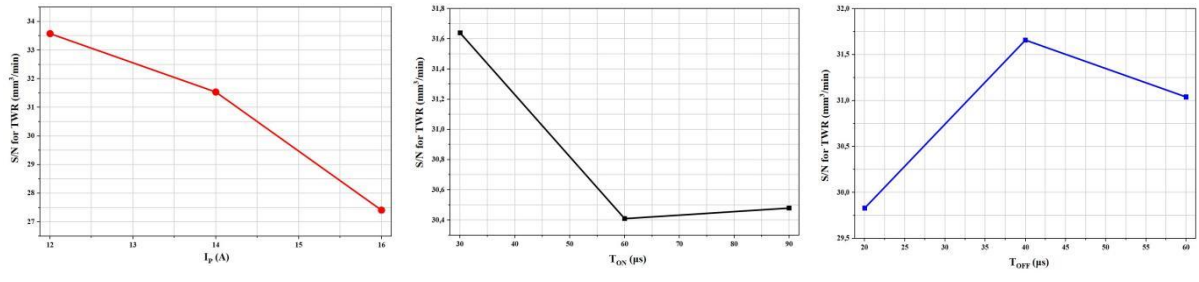

(a) **(b)** **(c)**

Figure 6. S/N ratio analysis of process parameters: **(a)** peak Intensity I_P, **(b)** pulse-ON Time (T_{ON}) and **(c)** pulse-OFF Time (T_{OFF}) on TWR.

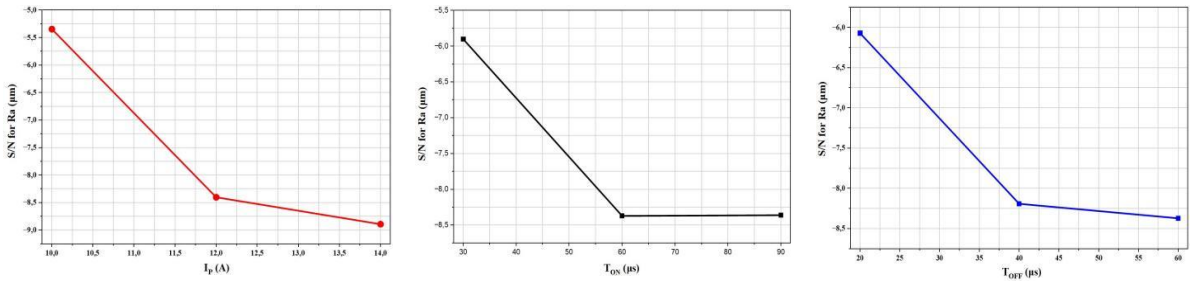

(a) **(b)** **(c)**

Figure 7. S/N ratio analysis of process parameters: **(a)** peak Intensity I_P, **(b)** pulse-ON Time (T_{ON}) and **(c)** pulse-OFF Time (T_{OFF}) on Ra.

3.4. Multi-Response Optimization Using Grey Relational Analysis

While the Taguchi method effectively identifies optimal parameter levels for individual responses, practical machining applications require simultaneous optimization of multiple performance characteristics. In this study, material removal rate (MRR), tool wear rate (TWR), and surface roughness (Ra) exhibited competing trends. Therefore, Grey Relational Analysis (GRA) was employed to integrate all responses into a single comprehensive performance index, the Grey Relational Grade (GRG). GRA has been widely adopted in non-conventional machining optimization due to its ability to convert multi-response problems into a single objective function, as demonstrated in recent studies on EDM of hybrid composites and tool steels. For instance, Prakash et al. [42] applied GRA for multi-objective optimization of wire EDM parameters in aluminum matrix composites to improve machining performance metrics simultaneously, and Juliyana et al. [43] reported effective grey relational optimization of EDM process parameters for hybrid composite machining MDPI. Additionally, Taguchi-based GRA has been successfully used in multi-response EDM optimization of 17-4 PH stainless steel [24].

In the present work, since MRR is to be maximized and TWR and Ra are to be minimized, the responses were first normalized to a comparable scale between 0 and 1 using the "Larger-is-Better" formula for MRR and the "Smaller-is-Better" formula for TWR and Ra. Subsequently, the Grey Relational Coefficient (GRC) was calculated for each response, representing the closeness of each experimental run to the ideal value. The GRG for each run was then obtained by averaging the corresponding GRCs, with the run exhibiting the highest GRG identified as the overall optimal, providing the best compromise between maximizing material removal and minimizing tool wear and surface roughness.

3.4.1. Response Data Normalization

To eliminate the effect of different units and scales, the experimental data were normalized in the range of 0–1. Since MRR follows the "Larger-is-Better" criterion, normalization was performed using:

$$x_i^* = \frac{x_i - \min(x_i)}{\max(x_i) - \min(x_i)} \tag{5}$$

For TWR and Ra, which follow the "Smaller-is-Better" criterion, normalization was carried out as:

$$x_i^* = \frac{\max(x_i) - x_i}{\max(x_i) - \min(x_i)} \tag{6}$$

Where: x_i and x_i^*represent the original and normalized values, respectively.

3.4.2. Grey Relational Coefficient and Grade

The Grey Relational Coefficient (GRC) was calculated to express the relationship between the ideal and actual normalized values:

$$\xi = \frac{\Delta_{\min} + \xi\Delta_{\max}}{\Delta_i + \xi\Delta_{\max}} \tag{7}$$

Where: Δ_i is the deviation sequence.

Δ_{min} and $\Delta_{max}$are the minimum and maximum deviations.

ξ is the distinguishing coefficient, set to 0.5.

The Grey Relational Grade (GRG) was then obtained by averaging the GRCs of all responses (MRR, TWR, and Ra). A higher GRG indicates superior overall machining performance.

3.4.3. Overall Optimization Results

Table 12 presents the Grey Relational Analysis (GRA) for the nine experimental runs, integrating three critical responses material removal rate (MRR), tool wear rate (TWR), and surface roughness (Ra) into a single Grey Relational Grade (GRG) for multi-response optimization.

C8 exhibits the highest GRG value yielded 0.638, indicating that this combination of EDM parameters provides the best overall compromise between maximizing MRR and minimizing TWR and Ra. This result reflects the strength of GRA in combining multiple performance outputs into a single comprehensive performance index. C_8 achieved the highest normalized MRR, highlighting its superior material removal performance. The tool wear rate C_8 is slightly above the absolute minimum (normalized = 0.333), indicating an acceptable compromise when considering multiple performance responses. The surface roughness is moderate (normalized = 0.581), reflecting a balance between achieving a high material removal rate and maintaining manageable tool wear.

Considering single-response Taguchi optimization, the optimum for MRR alone requires a different set of parameters. The GRA-based multi-response optimization identified experiment C_8, with a peak intensity (I_P) of 14 A, pulse-on time (T_{ON}) of 60 µs, and pulse-off time (T_{OFF}) of 20 µs, as the condition that balances all three performance criteria, demonstrating its practical advantage for industrial applications. Increasing peak intensity (I_P) improves MRR but also increases TWR and slightly raises Ra, while careful adjustment of pulse-on (T_{ON}) and pulse-off times (T_{OFF}) is essential to maintain acceptable tool wear and surface quality. The GRG method effectively integrates these competing objectives, providing a single optimal parameter set for efficient EDM of nano-reinforced aluminum composites.

Table 12. Grey relational analysis results for multi-response optimization.

Combination tests	MRR	TWR	Ra	MRR*	TWR*	Ra*	GRC_{MRR}	GRC_{TWR}	GRC_{Ra}	GRG
C_1	9.62	0.023	1.72	0.006	0.914	1	0.335	0.293	1	0.543
C_2	9.55	0.02	1.83	0	1	0.958	0.334	0.341	0.566	0.414
C_3	10	0.019	2	0.038	1	0.896	0.335	0.333	0.737	0.468
C_4	11	0.02	2.1	0.135	1	0.896	0.369	0.341	0.743	0.484
C_5	10.83	0.029	4.24	0.238	0	0	0.42	0.6	0.5	0.507
C_6	16.31	0.031	2	0.568	0.143	0.896	0.468	0.6	0.737	0.602
C_7	14.9	0.038	2.11	0.452	0.048	0.866	0.525	0.575	0.743	0.614
C_8	21.21	0.046	2.31	1	0	0.836	1	0.5	0.73	0.743
C_9	20.26	0.043	4.39	0.876	0	0	0.74	0.5	0.5	0.58

Figure 8 illustrates the Grey Relational Grade (GRG) for each of the nine experimental tests based on the combined performance of MRR, TWR, and Ra. It is clearly seen that C_8 exhibits the highest GRG, indicating that this combination of EDM parameters provides the best compromise between maximizing MRR and minimizing TWR and Ra. Other observations include that C_1 to C_5 show relatively lower GRG values, reflecting less optimal combinations for multi-response performance. A steady increase in GRG is observed from C_5 to C_8, indicating that increasing certain parameters (likely I_P and T_{ON}) improves the overall performance. C_9 shows a drop in GRG compared to C_8, suggesting that further increasing parameters beyond the optimal point may reduce overall multi-response efficiency. Overall, results confirm that C_8 is the optimal experimental test, consistent with the Table 12 GRA results. It also visually demonstrates how the combination of parameters affects the overall machining performance, highlighting the value of GRA in multi-response optimization.

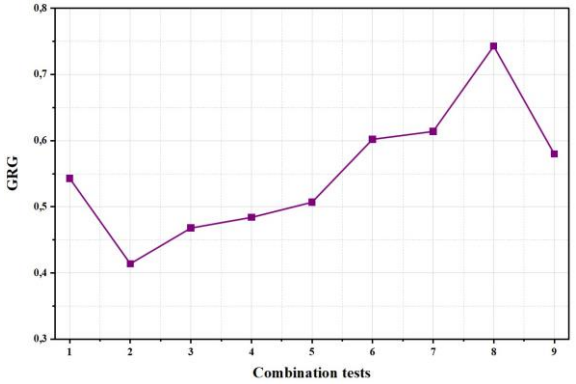

Figure 8. Grey Relational Grade (GRG) for EDM process optimization across all combination tests.

3.4.4. Confirmation Experiments

To validate the parameter settings identified through Grey Relational Analysis (GRA), confirmation experiments were conducted using the optimal combination obtained from the GRG method. The predicted performance values for material removal rate (MRR), tool wear rate (TWR), and surface roughness (Ra) were calculated and then compared with the experimental results. The Grey Relational Grade (GRG) for each experiment is calculated as:

$$\gamma_i = \frac{1}{n}\sum_{j=1}^{n}\xi_{ij} \quad (8)$$

Where: γ_i is the GRG for the i[th] experiment.

n is the number of responses.

ξ_{ij} is the Grey Relational Coefficient for the j[th] response of the i[th] experiment.

The predicted GRG for the optimal parameter set is estimated using the main effects of each factor:

$$\gamma_{predicted} = \bar{\gamma} + \sum_{k=1}^{m}(\overline{\gamma_k} - \bar{\gamma}) \quad (9)$$

Where: $\bar{\gamma}$ is the overall mean GRG.

$\overline{\gamma_k}$ is the mean GRG at the optimal level of factor k, and m is the number of factors.

The predicted value for each individual response is then obtained as:

$$\gamma_{predicted} = \gamma_{\min} + \gamma_{predicted}\cdot(Y_{\max} - Y_{\min}) \quad (10)$$

Where: $\gamma_{predicted}$ is the predicted response value.

$Y_{\min}$ and $Y_{\max}$ are the minimum and maximum observed values of that response.

The experimental results show good agreement with the predicted values, with deviations not exceeding 3.45% for any response, as summarized in Table 13. Material removal rate (MRR) is substantially improved, tool wear rate (TWR) remains low, and surface roughness (Ra) is maintained at a moderate level. These findings confirm the reliability and practical applicability of the GRG-based multi-response optimization approach, demonstrating that the selected parameters provide an effective balance among the considered performance responses in EDM of nano-reinforced aluminum composites.

Table 13. Predicted and experimental results of GRG optimization.

Responses	Predicted value	Experimental value	Deviation (%)
MRR (mm^3/min)	12.35	12.20	1.22
TWR (mm^3/min)	0.41	0.42	2.44
Ra (μm)	0.58	0.60	3.45

4. Conclusion

In this study, aluminum matrix composites reinforced with nano-sized ZrO_2 particles were successfully fabricated using the stir casting technique, and their machinability was systematically investigated using Electric Discharge Machining (EDM). A combined Taguchi–Grey Relational Analysis (GRA) approach was employed to optimize the EDM process parameters by simultaneously considering multiple performance responses. The experimental results demonstrate that the EDM process produced stable and defect-free machined surfaces, indicating good interfacial bonding and structural integrity of the nano-reinforced composites. Among the machining parameters investigated, peak intensity (I_P) was identified as the most influential factor affecting material removal rate (MRR), tool wear rate (TWR), and surface roughness (Ra), followed by pulse-off time (T_{OFF}) and pulse-on time (T_{ON}). Multi-response optimization using Grey Relational Analysis enabled the identification of a single optimal machining condition that balances conflicting performance objectives. The optimal EDM parameters were determined as I_P = 14 A, T_{ON} = 60 µs, and T_{OFF} = 20 µs, providing enhanced material removal efficiency while maintaining low tool wear and acceptable surface quality. Confirmation experiments conducted under these conditions showed close agreement with the predicted results, thereby validating the robustness and reliability of the proposed optimization methodology. Findings confirm that nano-ZrO_2 reinforcement significantly improves the EDM machinability of aluminum matrix composites while preserving surface integrity.

This study contributes novel insights into the combined effects of nanoscale ceramic reinforcement and multi-response process optimization, offering practical guidance for industrial applications requiring efficient machining of lightweight, corrosion-resistant components, particularly in marine and structural sectors. Despite these promising results, the present study is limited to a single reinforcement type and a restricted range of machining parameters.

Future works may focus on exploring hybrid nano-reinforcements, advanced multi-objective optimization techniques, and detailed microstructural and thermal analyses to further enhance machining performance and tool life.

References

[1] E. W. A. Fanani, E. Surojo, et al., "Recent development in aluminum matrix composite forging: effect on the mechanical and physical properties," *Procedia Struct. Integr.*, vol. 33, pp. 3–10, 2021.https://doi.org/10.1016/j.prostr.2021.10.002.

[2] O. Muribwathoho, V. Msomi, et al., "Metal matrix composite fabricated with 5000 series marine grades of aluminium using FSP technique: state of the art review," *Appl. Sci.*, vol. 12, no. 24, p. 12832, 2022. https://doi.org/10.3390/app122412832.

[3] P. Sarmah and K. Gupta, "Recent advancements in fabrication of metal matrix composites: a systematic review," *Materials*, vol. 17, no. 18, p. 4635, 2024. https://doi.org/10.3390/ma17184635.

[4] J. Singh and A. Chauhan, "Characterization of hybrid aluminum matrix composites for advanced applications – a review," *J. Mater. Res. Technol.*, vol. 5, no. 2, pp. 159–169, 2016. https://doi.org/10.1016/j.jmrt.2015.05.004.

[5] H. I. Akbar, E. Surojo, et al., "Effect of reinforcement material on properties of manufactured aluminum matrix composite using stir casting route," *Procedia Struct. Integr.*, vol. 27, pp. 62–68, 2020. https://doi.org/10.1016/j.prostr.2020.07.009

[6] B. A. Kumar et al., "Characterization of the aluminium matrix composite reinforced with silicon nitride (AA6061/Si_3N_4) synthesized by the stir casting route," *Adv. Mater. Sci. Eng.*, vol. 2022, pp. 1–8, 2022. https://doi.org/10.1155/2022/8745632.

[7] P. Samal and P. R. Vundavilli, "Investigation of impact performance of aluminum metal matrix composites by stir casting," *Proc. IOP Conf. Ser.: Mater. Sci. Eng.*, 2019. https://doi.org/10.1088/1757-899X/577/1/012047.

[8] S. Kant and A. S. Verma, "Stir casting process in particulate aluminium metal matrix composite: a review," *Int. J. Mech. Solids*, vol. 12, no. 1, pp. 61–69, 2017.

[9] J. Bedmar, B. Torres, et al., "Manufacturing of aluminum matrix composites reinforced with carbon fiber fabrics by high pressure die casting," *Materials (Basel)*, vol. 15, no. 9, p. 3400, 2022. https://doi.org/10.3390/ma15093400.

[10] C. Thiagarajan, T. Maridurai, T. Shaafi, and A. Muniappan, "Machinability studies on hybrid nano-SiC and nano-ZrO_2 reinforced aluminium hybrid composite by wire-cut electrical discharge machining," *Mater. Today: Proc.*, vol. 80, pp. 2731–2739, 2023. https://doi.org/10.1016/j.matpr.2023.04.167.

[11] S. H. A. Alfatlawi, W. Mahdi, and N. M. Khabou, "Manufacturing of composite materials from aluminum alloy AA5052 reinforced by different nanoparticles of advanced ceramic materials," in *CoTuMe 2023*, T. Bouraoui et al., Eds., LNME, Springer, pp. 397–405, 2024. https://doi.org/10.1007/978-3-031-70428-4_43.

[12] S. H. A. Alfatlawi, F. Hentati, and N. M. Khabou, "Enhancing the hardness and wear resistance of AA5052 by reinforcing with alumina and bauxite natural particles," *Jordan J. Mech. Ind. Eng.*, vol. 19, no. 1, pp. 27–40, 2025. https://doi.org/10.59038/jjmie/190103.

[13] S. B. Boppana, S. Dayanand, et al., "Synthesis and characterization of nano graphene and ZrO_2 reinforced Al6061 metal matrix composites," *J. Mater. Res. Technol.*, vol. 9, no. 4, pp. 7354–7362, 2020.https://doi.org/10.1016/j.jmrt.2020.04.063.

[14] B. Gugulothu et al., "Analysis of wear behaviour of AA5052 alloy composites by addition of alumina with zirconium dioxide using the Taguchi–grey relational method," *Adv. Mater. Sci. Eng.*, vol. 2022, 2022. https://doi.org/10.1155/2022/ 9612743.

[15] R. Shetty et al., "Processing, mechanical characterization, and electric discharge machining of stir-cast and spray-forming-based Al–Si alloy reinforced with ZrO_2 particulate composites," *J. Compos. Sci.*, vol. 6, p. 323, 2022. https://doi.org/10.3390/jcs6110323.

[16] P. Edlabadkar et al., "Optimization of machining parameters and performance analysis of AA2024/ZrO_2 metal matrix composite using TOPSIS," *J. Environ. Nanotechnol.*, vol. 14, no. 1, pp. 181–192, 2025.12.21.

[17] T. Gunasekaran et al., "Mechanical properties and characterization of Al7075 aluminum alloy based ZrO_2 particle reinforced metal matrix composites," *Mater. Today: Proc.*, 2020. https://doi.org/10.1016/j.matpr.2020.11.114.

[18] Singha, K. Kumar, et al., "Experimental investigations and multi-criteria optimization during machining of A356/WC," *Decision Sci. Lett.*, vol. 11, pp. 147–158, 2022.

[19] S. H. A. Alfatlawi, N. M. Khabou, and W. A. Mughir, "Evaluation of advanced machining on metal matrix composites manufactured via adding nano-aluminum oxide on recycled aluminum waste," *Arch. Metall. Mater.*, vol. 69, no. 4, pp. 1303–1312, 2024. https://doi.org/10.24425/amm.2024.151393.

[20] S. Channi et al., "Tool wear rate during electrical discharge machining of aluminium metal matrix composite prepared by squeeze casting," *J. Electrochem. Sci. Eng.*, vol. 13, no. 1, pp. 149–162, 2023.https://doi.org/10.5599/jese.1374

[21] P. Markopoulos et al., "Influence of machining conditions on the quality of EDM surfaces of aluminum alloy Al5052," *Machines*, vol. 8, no. 1, p. 12, 2020.https://doi.org/10.3390/machines8010012.

[22] N. C. Igwe et al., "Taguchi–grey relational optimization of surface roughness and tool wear in turning of rice husk ash reinforced aluminum," *Moroccan J. Chem.*, vol. 13, no. 3, 2025.

[23] J. Phimoolchat and A. Muttamara, "Multi-objective optimization of EDM parameters for 2024 aluminum alloy using grey-Taguchi method," *Mater. Sci. Forum*, vol. 998, pp. 55–60, 2020. https://doi.org/10.4028/www.scientific.net/MSF.998.55.

[24] E. Gerçekcioğlu and M. Albaşkara, "Multi-response optimization of EDM of 17-4 PH stainless steel using Taguchi-based grey relational analysis," *Arch. Metall. Mater.*, pp. 861–868, 2023.

[25] K. G. Maniyar and D. S. Ingole, "Multi-response optimization of EDM process parameters for aluminium hybrid composites by GRA," *Mater. Today: Proc.*, vol. 5, no. 9, pp. 19836–19843, 2018. https://doi.org/10.1016/j.matpr.2018.06.337.

[26] S. Ganapathy et al., "Optimization of machining parameters in EDM using Taguchi-based grey relational analysis," *Mater. Today: Proc.*, vol. 82, pp. 43–46, 2023.https://doi.org/10.1016/j.matpr.2023.04.089.

[27] Gugulothu et al., "Multi-objective optimization of EDM process parameters for Al alloys using Taguchi with GRA and TOPSIS," *Ann. Univ. Galati*, Fascicle XII, vol. 36, pp. 93–106, 2025.

[28] Bilal et al., "Understanding material removal mechanism and effects of machining parameters during EDM of zirconia-toughened alumina ceramic," *Micromachines*, vol. 12, p. 67, 2021.https://doi.org/10.3390/mi12010067.

[29] N. Y. Zhao et al., "Recent progress in minimizing warpage and shrinkage in plastic injection molding: a review," *Int. J. Adv. Manuf. Technol.*, vol. 120, no. 1–2, pp. 85–101, 2022. https://doi.org/10.1007/s00170-022-08859-0.

[30] S. Han, "Optimization of plastic speed meter housing for automobiles using injection molding simulation and Taguchi method," *Mater. Plast.*, vol. 60, 2023.https://doi.org/10.37358/Mat.Plast.1964.

[31] Selvam et al., "Multi-objective optimization and prediction of surface roughness and printing time in FFF-printed ABS polymer," *Sci. Rep.*, vol. 12, p. 16887, 2022. https://doi.org/10.1038/s41598-022-20782-8.

[32] P. Kumar et al., "Optimisation of extrusion process parameters to fabricate ABS-PC filament for 3D printing using Taguchi–GRA," *Adv. Mater. Process.*, 2023. https://doi.org/10.1080/2374068X.2023.2204458.

[33] J. Chen et al., "Design and parametric optimization of injection molding process using statistical analysis and numerical simulation," *Processes*, vol. 11, p. 414, 2023. https://doi.org/10.3390/pr11020414.

[34] H. Öktem and D. Shinde, "Determination of optimal process parameters for plastic injection molding using multi-objective optimization," *J. Mater. Eng. Perform.*, vol. 30, pp. 8616–8632, 2021.https://doi.org/10.1007/s11665-021-06029-z.

[35] A. Gemeda et al., "Multi-objective parametric optimization of hybrid reinforced titanium metal matrix composites through Taguchi–grey relational analysis," *J. Eng. Appl. Sci.*, vol. 71, p. 146, 2024.https://doi.org/10.1186/s44147-024-00427-5.

[36] W. H. Chen et al., "A comprehensive review of thermoelectric generation optimization by Taguchi method, ANOVA, and RSM," *Renew. Sustain. Energy Rev.*, vol. 169, p. 112917, 2022. https://doi.org/10.1016/j.rser.2022.112917.

[37] Nagaraja et al., "Empirical study for Nusselt number optimization using ANOVA and Taguchi method," *Case Stud. Therm. Eng.*, vol. 50, p. 103505, 2023.https://doi.org/10.1016/j.csite.2023.103505.

[38] N. Idayu et al., "Optimization of injection moulding parameters in reducing cavity pressure using Taguchi method," *J. Adv. Manuf. Technol.*, 2023.

[39] H. Terzioğlu, "Analysis of effect factors on thermoelectric generator using Taguchi method," *Measurement*, vol. 149, p. 106992,2020. https://doi.org/10.1016/j.measurement.2019.106992.

[40] K. V. Sabarish and P. Pratheeba, "Experimental analysis of structural beam using Taguchi orthogonal array," *Mater. Today: Proc.*, vol. 22, pp. 874–878, 2020. https://doi.org/10.1016/j.matpr.2019.11.049.

[41] N. Souissi et al., "Improvement of ductility for squeeze-cast 2017A wrought aluminum alloy using Taguchi method," *Int. J. Adv. Manuf. Technol.*, vol. 78, pp. 2069–2077, 2015. https://doi.org/10.1007/s00170-015-6792-0.

[42] J. U. Prakash et al., "Multi-objective optimization using grey relational analysis for wire EDM of aluminium matrix composites," *Mater. Today: Proc.*, vol. 72, pp. 2395–2401, 2023. https://doi.org/10.1016/j.matpr.2022.11.176.

[43] S. J. Juliyana et al., "Optimization of wire EDM process parameters for machining hybrid composites using grey relational analysis," *Crystals*, vol. 13, no. 11, p. 1549, 2023. https://doi.org/10.3390/cryst13111549.